Journal of Sound and Vibration (2002) **254**(5), 1012–1024
doi:10.1006/jsvi.2001.4106, available online at http://www.idealibrary.com on IDEAL®

COMPARISON OF DIFFERENT MODELLING TECHNIQUES TO SIMULATE THE VIBRATION OF A CRACKED ROTOR

H. KEINER AND M. S. GADALA

Department of Mechanical Engineering, The University of British Columbia, Vancouver, BC, Canada V6T 1Z4. E-mail: gadala@mech.ubc.ca

(*Received* 30 *January* 2001, *and in final form* 10 *September* 2001)

1. INTRODUCTION

Large-scale rotating machinery, such as turbines, generators or drums, often develop fatigue cracks throughout their service life, which can severely damage machine components or even lead to catastrophic failure. In general, non-destructive testing is used in inspection intervals to prevent such failures, but recently vibration analysis has received much attention in trying to continuously monitor the machine's condition. The advantages of on-line condition monitoring are early warnings of machine failure and reduced downtime.

The vibration of a cracked shaft has been investigated by many researchers. Extensive reviews of the literature on this topic have been compiled by Wauer [1] and more recently by Dimarogonas [2]. In general, a slight decrease and splitting of the first natural frequency, resonance at half the first natural frequency, a slight increase in the 1/rev. and 3/rev. harmonic responses and a strong increase in the 2/rev. harmonic response are referred to as key indicators for a transverse crack in a shaft [3–5]. These observations have been confirmed in experimental studies [5–7]. The results have been implemented in crack detection systems in industry [4, 8]. There have been several incidents where vibration monitoring led to the detection of a crack preventing catastrophic failure [9–11].

Until today, the greatest difficulty in crack detection and identification remains the quantitative evaluation of the crack parameters and the distinction between a developing crack from other faults such as imbalance, misalignment, shaft bow, bearing failure, etc. [8, 11]. The key issues in developing an accurate modelling technique of a cracked rotor are the reduced stiffness of the cracked cross-section, the variation of stiffness over one revolution due to the opening and closing of the crack (crack breathing) and the complexity in geometry of the rotor, in particular in the region of the developing crack. Dimarogonas [2] developed an analytical expression for the additional local crack compliance for a six-degree-of-freedom cracked beam segment. Alternatively, the local compliance matrix can be determined through a 3-D static finite element (FE) analysis [4, 12, 13]. The crack breathing mechanism has been modelled in a variety of ways, all resulting in a time-varying local compliance matrix, which is incorporated into the dynamic equations for the rotor [12, 14]. The equations of motion have been solved analytically [6], in a linearized form [5], or numerically through time-integration from the initial conditions [4, 12, 15].

In most cases, the geometry of the rotor has been limited to a simple Laval rotor model and a single transverse crack placed at various locations along the axis. Sekhar [16] and Tsai and Wang [17] analyzed the behaviour of a rotor containing more than one crack. Sekhar [15] also investigated the influence of a slanted crack in a shaft. Researchers using

0022-460X/02/$35.00

the Finite Element Method used beam elements of various dimensions and concentrated masses along the shaft axis to model stepped shafts and turbine discs [4, 15]. However, it becomes difficult to vary the location of the crack since every relocation into a shaft segment of different geometry requires the development of a new cracked beam element. In particular, a crack in a non-cylindrical rotor segment, such as blades or spokes, and areas of stress concentrations render the previously developed cracked beam elements invalid. This problem has not yet been addressed in the literature.

2. THEORY

A simple cracked shaft with a heavy mass at midspan is shown in Figure 1(a). Vibration of the shaft under pure gravity load is caused by the changing stiffness of the shaft depending on whether the crack lies in the tensile or compressive region of axial normal stress. The periodic opening and closing of the crack is called "crack breathing".

2.1. ANALYTICAL CRACK FORCE METHOD

The analytical approach is based on the simplified two-degree-of-freedom model shown in Figure 1(b). The equations of motion for this model can be written as

$$\mathbf{M}\ddot{x} + \mathbf{C}\dot{x} + \mathbf{K}x = F, \tag{1}$$

where

$$\mathbf{M} = \begin{bmatrix} m & 0 \\ 0 & m \end{bmatrix}, \quad \mathbf{C} = \begin{bmatrix} c & 0 \\ 0 & c \end{bmatrix}, \quad \mathbf{K}(x, \Omega t) = \begin{bmatrix} k_{xx}(x, \Omega t) & k_{xy}(x, \Omega t) \\ k_{yx}(x, \Omega t) & k_{yy}(x, \Omega t) \end{bmatrix},$$

$$F = \begin{bmatrix} 0 \\ -mg \end{bmatrix}, \quad x = \begin{bmatrix} x \\ y \end{bmatrix},$$

and where Ω is the rotational velocity.

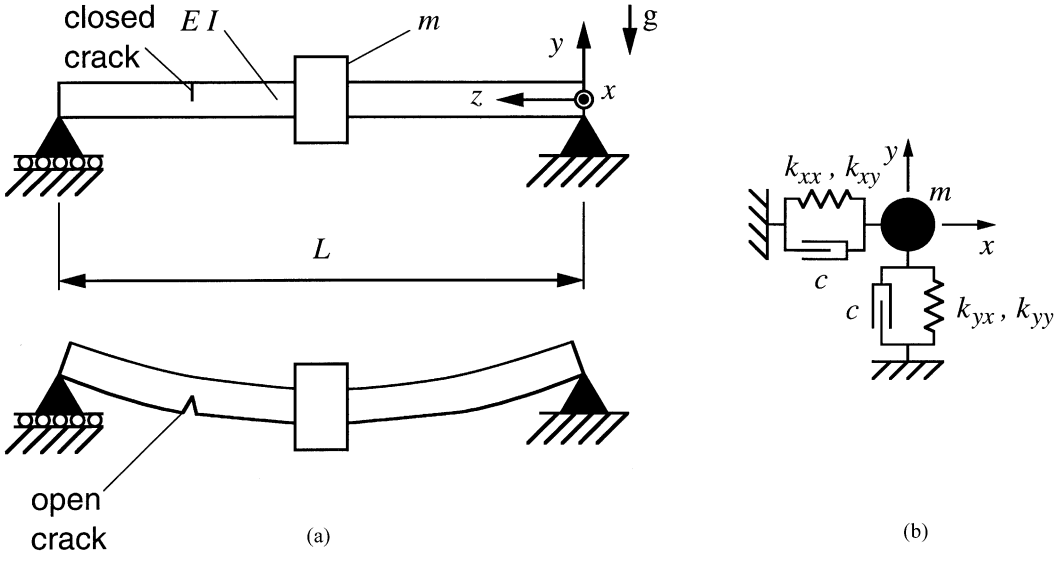

Figure 1. Cracked Laval rotor under gravity load. (a) The crack will be closed when the crack faces are in compression, open when the crack faces are in tension. (b) Two-degree-of-freedom analytical model of a cracked shaft.

Equation (1) can be linearized under the assumption of dominant static deflection and by decomposing **K** into a constant component of the uncracked structure, $\mathbf{K}_0$, and a variable component due to crack breathing, $\Delta\mathbf{K}(\Omega t)$, yielding [5]

$$\Rightarrow \mathbf{M}\ddot{x} + \mathbf{C}\dot{x} + \mathbf{K}_0 x = F + \Delta\mathbf{K}(\Omega t)x_{static}, \tag{2}$$

where x_{static} is the static deflection of the uncracked shaft.

The term $\Delta\mathbf{K}(\Omega t)\, x_{static}$ is called the "crack force" and can be Fourier transformed into the harmonics of the rotational speed:

$$\Rightarrow \mathbf{M}\ddot{x} + \mathbf{C}\dot{x} + \mathbf{K}_0 x = F + \sum_{k=0}^{\infty} A_k \cos(k\Omega t) + B_k \sin(k\Omega t). \tag{3}$$

The method represents a very efficient way of approximating the vibration of a cracked rotor. However, it is confined to the analysis of one-dimensional (1-D) beam models.

2.2. THREE-DIMENSIONAL TRANSIENT ANALYSIS

To avoid the assumptions made above regarding the shaft and crack geometry, local crack compliance, crack breathing mechanism and dominant static deflection, the only viable alternative is a transient analysis using 3-D solid finite elements. Figure 2 shows an FE model of a cracked shaft segment using eight-noded brick elements. The crack face

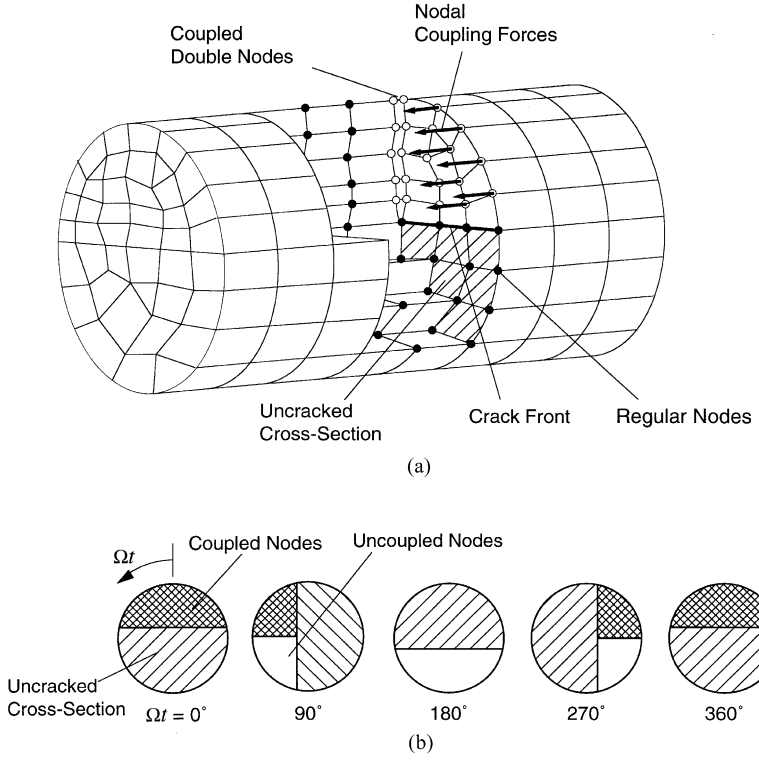

Figure 2. 3-D FE model of a cracked shaft segment. (a) Double nodes are used to model the crack faces. The nodes are coupled when the crack is closed, uncoupled when it is open. The nodal coupling forces represent the load transfer across the crack faces. (b) Uncoupling and re-coupling of nodes is used to simulate crack breathing over one revolution.

surfaces are modelled using double nodes which are identical in location but topologically belong either to the right or the left crack face. When all crack face nodes are coupled, the model is identical to the uncracked shaft, and the depicted nodal coupling forces represent the load transfer across the crack faces. Therefore, the closed crack is modelled by coupling the double nodes giving the rotor compressive stiffness over the crack faces, while the open crack is modelled by removing the coupling bonds allowing the crack faces to gap. The analysis is performed through time-integration from the initial conditions, e.g., nominal rotational velocity and static deflection of the shaft, with the crack being fully closed in the compressive region. The main drawback is that 3-D solid FE models of rotors can be very large and computations become quite extensive making it an unfeasible solution procedure for on-line crack identification purposes. Furthermore, problems of stability for explicit or convergence problems for implicit time-integration schemes pose additional difficulties.

2.3. THE NODAL CRACK FORCE APPROACH

In order to combine the advantages of the simple solution scheme for the analytical crack force approach with the versatility in rotor and crack geometry of the 3-D transient analysis, a new approach is introduced labelled as the 3-D nodal crack force approach. In this approach, the same FE model is used as in the transient analysis, shown in Figure 2(a), containing the coupled double nodes at the crack faces. However, the crack breathing mechanism is approximated by nodal crack forces under the assumption of dominant static deflection. The uncracked rotor is analyzed under steady state conditions for the applied load at various angles of rotation, and the resulting nodal coupling forces are recorded. Since it is irrelevant if the crack face nodes are indeed coupled or if the coupling forces are known *a priori* and are applied as external forces, it can be concluded that the steady state solutions for both cases are indentical.

For the breathing crack, the coupled nodal forces exist when the crack is closed and the crack faces are in compression, but they are missing when the crack is open and the crack faces are in tension. This effect can be achieved by adding a time-dependent nodal crack force as external load to the crack face nodes which will be of equal magnitude but opposite direction of any tensile nodal coupling force while being zero at times when the nodal coupling force is compressive; see Figure 3. Superposition of these two load cases results in a crack breathing mechanism which only transfers compressive load over the crack faces.

Practically, the FE model with all nodes coupled is analyzed in a steady state analysis at discrete points of angle of rotation under the applied load of the rotor, e.g., gravity. The nodal coupling forces are recorded as discrete function of the angle of rotation, $F_N^n = F_N^n(\Omega t)$, and the nodal crack forces are computed by

$$F_C^n(\Omega t) = \begin{cases} -F_N^n(\Omega t), & F_N^n(\Omega t) \geqslant 0, \\ 0, & F_N^n(\Omega t) < 0, \end{cases} \tag{4}$$

where F_N^n is the recorded nodal coupling force, F_C^n the nodal crack force and n the node number of the crack face node.

The dynamic FE equations to be solved are

$$\mathbf{M}\ddot{u} + \mathbf{C}\dot{u} + \mathbf{K}u = F + F_N + F_C. \tag{5}$$

Note that the partial solution u_1, where $u_1 + u_2 = u$, of equation

$$\mathbf{M}\ddot{u}_1 + \mathbf{C}\dot{u}_1 + \mathbf{K}u_1 = F + F_N \tag{6}$$

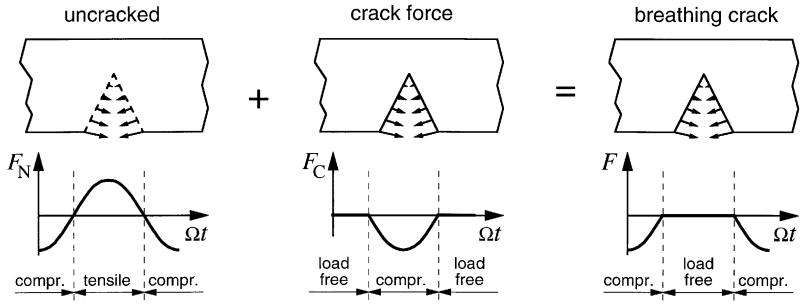

Figure 3. Superposition of the nodal crack forces used to simulate crack breathing.

is the solution to the uncracked rotor problem which has already been solved when obtaining the nodal coupling forces; thus only

$$\mathbf{M}\ddot{u}_2 + \mathbf{C}\dot{u}_2 + \mathbf{K}u_2 = F_C \tag{7}$$

needs to be solved to find the combined solution u.

2.4. SOLVING THE FE EQUATIONS IN A ROTATING CO-ORDINATE SYSTEM

The equations of motion of the nodal mass m rotating around the origin in the stationary co-ordinate system (x, y, z), see Figure 4, are given by

$$\mathbf{M}\ddot{u} + \mathbf{C}\dot{u} + \mathbf{K}(u + (\mathbf{I} - \mathbf{R})x_0) = F, \tag{8}$$

where

$$\mathbf{K}(\Omega t) = \mathbf{R}\mathbf{K}(\Omega t = 0)\mathbf{R}^{\mathrm{T}} = \mathbf{R}\mathbf{K}_0\mathbf{R}^{\mathrm{T}}, \quad \mathbf{R} = \begin{bmatrix} \cos\Omega t & -\sin\Omega t & 0 \\ \sin\Omega t & \cos\Omega t & 0 \\ 0 & 0 & 1 \end{bmatrix}.$$

Equation (8) can be transformed into the rotating co-ordinate system (ξ, η, z) by

$$x(\Omega t) = \mathbf{R}\xi \tag{9}$$

resulting in

$$u = \mathbf{R}\varepsilon + (\mathbf{R} - \mathbf{I})x_0 \tag{10}$$

for the displacement from m to m'.

Replacing u in equation (8) with the expression from equation (10) results in

$$\dot{u} = \dot{\mathbf{R}}\varepsilon + \mathbf{R}\dot{\varepsilon} + \dot{\mathbf{R}}x_0, \qquad \ddot{u} = \mathbf{R}\ddot{\varepsilon} + 2\dot{\mathbf{R}}\dot{\varepsilon} + \ddot{\mathbf{R}}\varepsilon + \ddot{\mathbf{R}}x_0, \tag{11}$$

$$\dot{\mathbf{R}} = \Omega\begin{bmatrix} -\sin\Omega t & -\cos\Omega t & 0 \\ \cos\Omega t & -\sin\Omega t & 0 \\ 0 & 0 & 0 \end{bmatrix}, \qquad \ddot{\mathbf{R}} = -\Omega^2\begin{bmatrix} \cos\Omega t & -\sin\Omega t & 0 \\ \sin\Omega t & \cos\Omega t & 0 \\ 0 & 0 & 0 \end{bmatrix} = -\Omega^2\tilde{\mathbf{R}}, \tag{12}$$

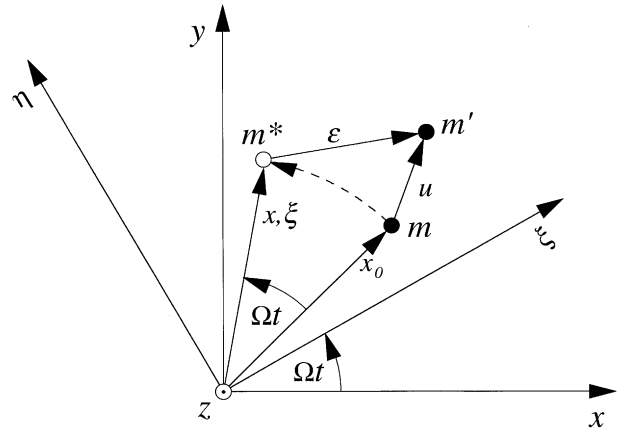

Figure 4. Displacement of a point mass m rotating about z in stationary and rotating co-ordinates; m^* denotes the unperturbed position of m at time t.

and finally,

$$\mathbf{M}\mathbf{R}\ddot{\varepsilon} + (2\mathbf{M}\dot{\mathbf{R}} + \mathbf{C}\mathbf{R})\dot{\varepsilon} + (\mathbf{K}\mathbf{R} - \Omega^2\mathbf{M}\tilde{\mathbf{R}} + \mathbf{C}\dot{\mathbf{R}})\varepsilon = F + \Omega^2\mathbf{M}\tilde{\mathbf{R}}x_0 - \mathbf{C}\dot{\mathbf{R}}x_0. \tag{13}$$

Pre-multiplying equation (13) with $\mathbf{R}^{\mathrm{T}}$ yields

$$\mathbf{R}^{\mathrm{T}}\mathbf{M}\mathbf{R}\ddot{\varepsilon} + (2\mathbf{R}^{\mathrm{T}}\mathbf{M}\dot{\mathbf{R}} + \mathbf{R}^{\mathrm{T}}\mathbf{C}\mathbf{R})\dot{\varepsilon} + (\mathbf{R}^{\mathrm{T}}\mathbf{K}\mathbf{R} - \Omega^2\mathbf{R}^{\mathrm{T}}\mathbf{M}\tilde{\mathbf{R}} + \mathbf{R}^{\mathrm{T}}\mathbf{C}\dot{\mathbf{R}})\varepsilon$$

$$= \mathbf{R}^{\mathrm{T}}F + \Omega^2\mathbf{R}^{\mathrm{T}}\mathbf{M}\tilde{\mathbf{R}}x_0 - \mathbf{R}^{\mathrm{T}}\mathbf{C}\dot{\mathbf{R}}x_0. \tag{14}$$

Under the assumption that mass and damping matrix are diagonal matrices of equal members, i.e., $\mathbf{M} = \mathrm{diag}(m, m, m)$ and $\mathbf{C} = \mathrm{diag}(c, c, c)$, equation (14) can be written as

$$\mathbf{M}\ddot{\varepsilon} + (2\mathbf{M}\mathbf{G} + \mathbf{C})\dot{\varepsilon} + (\mathbf{K}' - \Omega^2\tilde{\mathbf{M}} + \mathbf{C}\mathbf{G})\varepsilon = \mathbf{R}^{\mathrm{T}}F + \Omega^2\tilde{\mathbf{M}}x_0 - \mathbf{C}\mathbf{G}x_0, \tag{15}$$

where

$$\mathbf{K}' = \mathbf{R}^{\mathrm{T}}\mathbf{K}\mathbf{R} = \mathbf{K}_0, \quad \tilde{\mathbf{M}} = \mathrm{diag}(m, m, 0), \quad \mathbf{G} = \mathbf{R}^{\mathrm{T}}\dot{\mathbf{R}} = \Omega\begin{bmatrix} 0 & -1 & 0 \\ 1 & 0 & 0 \\ 0 & 0 & 0 \end{bmatrix}.$$

$\mathbf{K}'$ represents the constant stiffness matrix of the rotor in rotating co-ordinates and does not depend on Ωt; thus, equation (15) can be solved as a linear dynamic problem. The terms $\Omega^2\tilde{\mathbf{M}}\varepsilon$ and $\Omega^2\tilde{\mathbf{M}}x_0$ represent the centrifugal forces, $2\mathbf{M}\mathbf{G}\dot{\varepsilon}$ the Coriolis force, and $\mathbf{C}\mathbf{G}\varepsilon$ and $\mathbf{C}\mathbf{G}x_0$ the additional forces due to damping described in the rotating co-ordinate system.

The discrete set of nodal crack forces, $F_C(\Omega t)$, is transferred into rotating co-ordinates and Fourier transformed considering the first $p + 1$ terms:

$$\mathbf{R}^{\mathrm{T}}F_C(\Omega t) = \sum_{k=0}^{p} A_k \cos(k\Omega t) + B_k \sin(k\Omega t). \tag{16}$$

Replacing the applied load $\mathbf{R}^{\mathrm{T}}F$ in equation (15) with $\mathbf{R}^{\mathrm{T}}F_C$ yields

$$\mathbf{M}\ddot{\varepsilon} + (2\Omega\mathbf{MG} + \mathbf{C})\dot{\varepsilon} + (\mathbf{K}' - \Omega^2\tilde{\mathbf{M}} + \Omega\mathbf{CG})\varepsilon$$
$$= \Omega^2\tilde{\mathbf{M}}x_0 - \Omega\mathbf{CG}x_0 + A_0 + A_1\cos(\Omega t) + B_1\sin(\Omega t) + A_2\cos(2\Omega t) + B_2\sin(2\Omega t)$$
$$+ \cdots + A_p\cos(p\Omega t) + B_p\sin(p\Omega t). \tag{17}$$

The problem can now be solved in $p + 1$ linear harmonic response analyses and the solutions are superimposed:

$$\varepsilon = \varepsilon_0 + \varepsilon_1 + \cdots + \varepsilon_p, \quad u_2 = \mathbf{R}\varepsilon, \quad u = u_1 + u_2. \tag{18–20}$$

The computational savings of the nodal crack force approach over a complete transient analysis are tremendous. For example, if the uncracked steady state solution (u_1) and the nodal coupling forces (F_N) are evaluated in a series of linear analyses at an increment of 15° over one revolution, and the cracked vibration response is determined using the first six Fourier coefficients, the linear FE equations must be solved for a total of 30 times. In comparison, a transient analysis over four revolutions with an incremental step of 5° and approximately four iterations per step results in 1152 necessary solutions of the same equations. This yields a computational savings factor of approximately 40 : 1 for the nodal crack force approach, greater when symmetry can be used in determining the uncracked steady state solution. Furthermore, any re-evaluation of the cracked vibration response for a different set of parameters requires only the six dynamic linear analyses, as long as the uncracked steady state solution remains valid.

3. ANALYSIS AND RESULTS

Two example problems were solved to compare the two-degrees-of-freedom analytical (anal.) and 3-D transient FE (tran.) methods and to verify the validity of the nodal crack force (NCF) approach.

3.1. EXAMPLE 1—SHORT CANTILEVER SHAFT

Example 1 is a weightless cantilever shaft ($D = 40$ mm, $L = 100$ mm) under gravity load with a heavy mass ($m = 257$ kg) at its free end, as shown in Figure 5. The material properties used were those of aluminium ($E = 70$ GPa, $\nu = 0{\cdot}3$). No damping was considered throughout the analysis. A transverse crack was located at midspan and the crack length to shaft diameter ratio was $a/D = 0{\cdot}25$. The reduced stiffness due to the crack in the analytical model was computed using the method by Dimarogonas [2]. Crack breathing was simulated using the reduced stiffness of the fully open crack when the crack was in tension and the uncracked shaft stiffness otherwise. For the nodal crack force approach, the static deflection was calculated for one full revolution in increments of 15°, and the nodal coupling forces were recorded. The nodal crack forces and the analytical crack force were determined by Fourier analysis considering the first six terms. The transient analysis was performed using implicit time-integration and an incremental angle of rotation $\Delta\Omega t = 5°$ resulting in a time step size $\Delta t = \Delta\Omega t/\Omega$. Initial conditions were established by applying the external gravity load and displacement boundary conditions for an initial, small time step ignoring inertia effects. The solution was computed for four revolutions and in general, stabilized after 2–3 revolutions. All solutions for the 3-D FE model were obtained using the

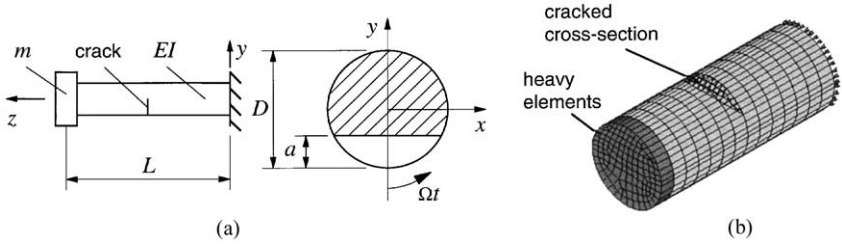

Figure 5. (a) Analytical and (b) 3-D FE model of a cantilever shaft with a transverse crack at midspan.

TABLE 1

Comparison of natural frequency and static deflection for a cantilever shaft in bending

Model	Static deflection (mm)	First natural frequency (Hz)		
		Uncracked	Cracked	
			Horizontal	Vertical
Analytical	0·085	53·8	53·4	50·5
3-D FEA	0·097	52·0	51·7	49·9

commercial FE code ANSYS [18]. Plotted displacements were made non-dimensional by dividing through the vertical static deflection from the FE analysis.

Table 1 lists the uncracked static deflection and natural frequencies for the analytical and the FE model. The resulting horizontal and vertical deflections for the quasi-static case, i.e., $\Omega/\omega_n = 0{\cdot}001$, ω_n being the lowest lateral natural frequency of the uncracked FE model, are shown in Figure 6. The horizontal deflection from the nodal crack force approach and the transient analysis show a slight discrepancy, while the vertical deflections are practically identical. The deflection based on the analytical model proves too flexible in both directions, which is due to the greater analytical compliance compared to 3-D FE results [12, 13].

The shaft orbits for rotational speeds of $\Omega/\omega_n = 0{\cdot}32$, 0·45 and 0·9 are shown in Figure 7. For $\Omega/\omega_n = 0{\cdot}9$, the rotational speed is close to the critical speed of the shaft; thus, the two orbits from the linearized solutions are dominated by a single loop due to the first harmonic excitation component of the crack forces. The transient solution shows a spiral from the initial conditions at the origin approximately to the size of the nodal crack force solution with each loop representing a full revolution of the shaft. The orbits for $\Omega/\omega_n = 0{\cdot}46$ exhibit the double loop, typically associated with the existence of a crack in a shaft rotating close to half its critical speed. Qualitatively, the orbit shapes from all methods are very similar, but quantitatively, the nodal crack force approach yields a slightly better match than the analytical solution.

3.2. EXAMPLE 2—LAVAL ROTOR

In example 2, a Laval rotor ($D = 25$ mm, $L = 2000$ mm) with point mass ($m = 20$ kg) at midspan under gravity load was considered; see Figure 8. The shaft was modelled with

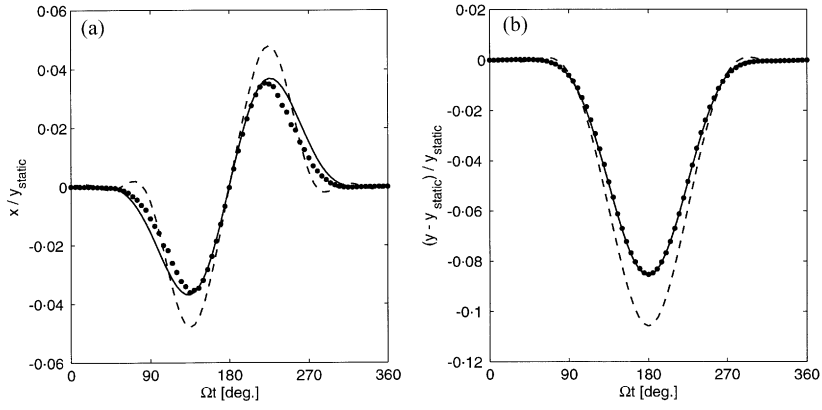

Figure 6. Non-dimensional, quasi-static (a) horizontal and (b) vertical displacement of a cracked cantilever shaft (–, NCF; - -, anal.; ● trans.).

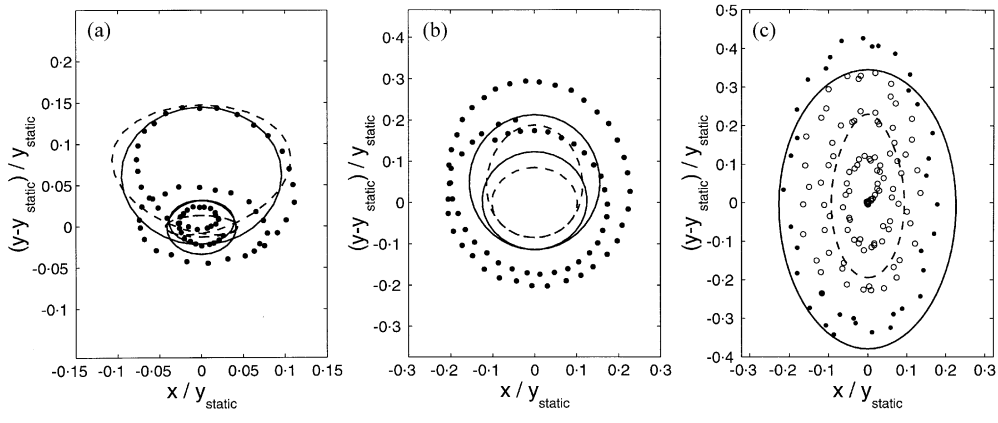

Figure 7. Non-dimensional orbits of a cantilever shaft for rotational speeds (a) $\Omega/\omega_n = 0{\cdot}32$, (b) 0·45 and (c) 0·9 (–, NCF; - -, anal.; ○, trans. first and second rev.; ●, trans. third rev.).

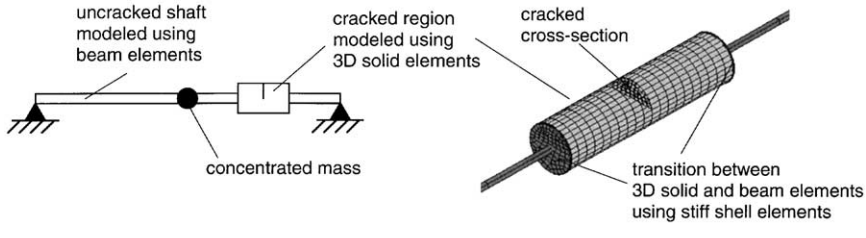

Figure 8. 3-D FE model of a simply supported Laval rotor with a transverse crack at quarter length.

simple support boundary conditions at both ends and the material properties of aluminium ($E = 70$ GPa, $\nu = 0{\cdot}3$). The crack was located at quarter length with $a/D = 0{\cdot}4$. In the FE model, only the region around the crack was modelled using eight-noded 3-D solid elements. The remainder of the shaft was modelled using two-noded Timoshenko beam elements with six degrees of freedom at each node. In the transition zone between beam and 3-D solid elements, very stiff four-noded shell elements overlaid the shaft cross-section,

TABLE 2

Comparison of natural frequency and static deflection for a Laval rotor in bending

Model	Static deflection (mm)	First natural frequency (Hz)		
		Uncracked	Cracked	
			Horizontal	Vertical
Analytical	1·523	12·8	12·6	12·1
3-D FEA	1·520	12·8	12·8	12·6

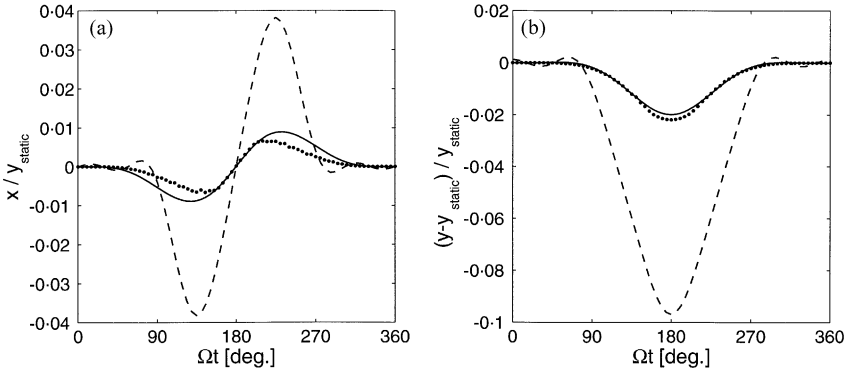

Figure 9. Non-dimensional quasi-static (a) horizontal and (b) vertical displacement of a cracked Laval rotor (–, NCF; - -, anal.; ●, trans.).

transferring the bending moment and providing the continuity of the shaft's slope. Damping was included and the modal damping factor was set to $\zeta = 0{\cdot}05$. The analysis process for both models was identical with that of the previous example.

Table 2 compares the natural frequencies and uncracked static deflection. The good agreement proves the validity of employing the shell elements for the transition between beam and 3-D solid elements. The resulting horizontal and vertical deflections for the quasi-static case, i.e., $\Omega/\omega_n = 0{\cdot}001$, is shown in Figure 9. Again, the results from the transient analysis and the nodal crack force approach are virtually identical, while the analytical solution exhibits much greater values due to the greater local crack compliance.

The vibration amplitude for various rotational speeds was computed and the results are shown in Figure 10. The additional peaks at 1/2 and 1/3 of the uncracked natural frequency due to the crack can be clearly identified. Overall vibration amplitudes from transient and nodal crack force analyses show good agreement while the analytical solution is significantly greater over the entire range of rotational speeds. Therefore, results from the analytical approach are ignored in the following comparison of orbits, shown in Figure 11. Quantitatively, the orbits show good agreement and seem to match more closely than the orbits of example 1. In particular, the transient solution seems more stable over the course of one revolution, which can be attributed to the damping and the diminishing effect of the initial conditions.

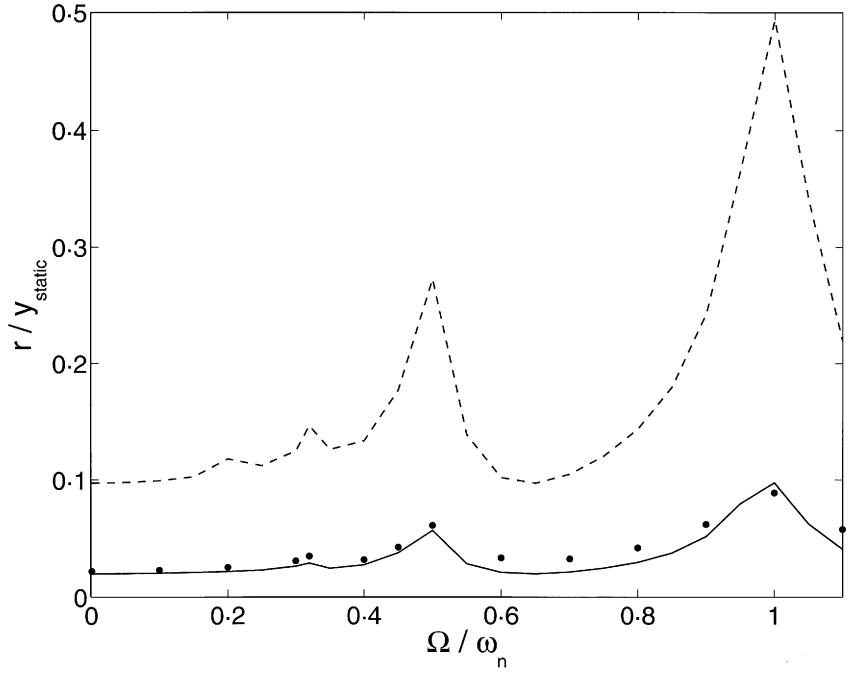

Figure 10. Comparison of the non-dimensional vibration amplitude r/y_{static}, where $r = \sqrt{x^2 + (y - y_{static})^2}$ over the sub-critical range (–, NCF; - -, anal.; ●, trans.).

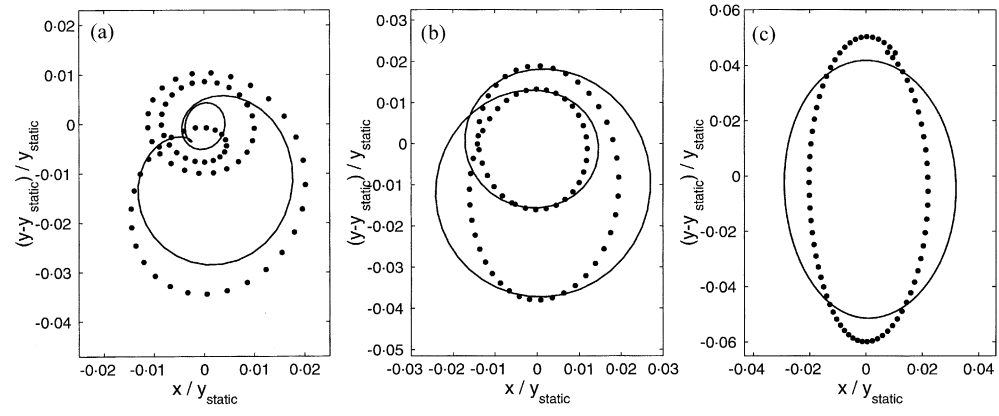

Figure 11. Non-dimensional shaft orbits of a Laval rotor for rotational speeds (a) $\Omega/\omega_n = 0{\cdot}32$, (b) 0·45 and (c) 0·9 (–, NCF; - -, anal.; ●, trans. third rev.).

4. CONCLUSIONS

A two-degrees-of-freedom analytical model, a linearized 3-D FE model and a non-linear transient 3-D FE model were used to predict the vibration of a cracked shaft under gravity. Due to the lack of experimental results for the specific cases presented here, the results from the 3-D transient analysis must be regarded as the most accurate since they include the non-linear effect of the crack breathing as well as the influence of the 3-D geometry. In almost all cases, a significant difference in vibration level predicted by the analytical model

compared to the 3-D FE models can be observed. This is primarily due to the less accurate analytical development of the local crack compliance. While this problem can be overcome by using static 3-D FE analysis to develop the crack compliance matrix, other necessary assumptions regarding the crack breathing behaviour and the problem of approximating a 3-D structure with a beam model remain. On the other hand, the nodal crack force approach exhibits excellent agreement with the transient analysis and uses a 3-D solid FE model, thus avoiding assumptions regarding rotor or crack geometry altogether. The only necessary assumption is the dominance of the uncracked steady state deflection, which is often the case in practice.

Another important criterion in evaluating each method is computational efficiency. While the effort for solving the equations of the much simplified analytical model is negligible, the nodal crack force method offered a computational performance benefit of 40 : 1 compared to the 3-D transient analysis. Subsequently, evaluating the vibration for different crack parameters results in an even greater computational advantage since the internal nodal crack forces do not have to be re-evaluated. Therefore, the authors believe that the approach will prove valuable in the process of on-line crack detection on rotors which cannot be well approximated by a beam model.

REFERENCES

1. J. WAUER 1990 *Applied Mechanics Review* **43**, 13–17. On the dynamics of cracked rotors: a literature survey.
2. A. D. DIMAROGONAS 1996 *Engineering Fracture Mechanics* **55**, 831–857. Vibration of cracked structures: a state of the art review.
3. D. E. BENTLY and A. MUSZYNSKA 1986 *Proceedings of the* 15*th Turbomachinery Symposium*, *Corpus Christi*, *U.S.A.*, 129–139. Detection of rotor cracks.
4. I. IMAM, S. H. AZZARO, R. J. BANKERT and J. SCHEIBEL 1989 *Journal of Vibration, Acoustics, Stress, and Reliability in Design* **111**, 241–250. Development of an on-line rotor crack detection and monitoring system.
5. M. LIAO and R. GASCH 1992 *International Conference on Vibration in Rotating Machinery*, *Bath*, *U.K.*, 289–295. Crack detection in rotating shafts—an experimental study.
6. C. A. PAPADOPOULOS and A. D. DIMAROGONAS 1988 *Journal of Vibration, Acoustics, Stress, and Reliability in Design* **110**, 1–8. Coupled longitudinal and bending vibrations of a cracked shaft.
7. A. TAMURA, Y. IWATA and H. SATO 1988 *International Conference on Vibration in Rotating Machinery*, *Edinburgh*, *U.K.*, 647–653. Unstable vibration of a rotor with a transverse crack.
8. J. R. SCHEIBEL, I. IMAM, T. G. EBBEN and R. BLOMGREN 1987 *Proceedings of the American Power Conference*, *Chicago*, *U.S.A.*, 369–380. An expert system-based, on-line rotor crack monitor for utility steam turbines.
9. A. F. P. SANDERSON 1992 *International Conference on Vibration in Rotating Machinery*, *Bath*, *U.K.*, 263–273. The vibration behaviour of a large steam turbine generator during crack propagation through the generator rotor.
10. V. BICEGO, E. LUCON, C. RINALDI and R. CRUDELI 1999 *Nuclear Engineering and Design* **188**, 173–183. Failure analysis of a generator rotor with a deep crack detected during operation: fractographic and fracture mechanics approach.
11. W. FRANKLIN, D. E. BENTLY, P. GOLDMAN and A. MUSZYNSKA 1997 *Pumping Machinery Symposium—Proceedings of the* 1997 *ASME Fluids Engineering Summer Meeting*, *Vancouver*, *Canada*. Early cracked shaft detection in pumps using rotor lateral vibration analysis.
12. B. DIRR and B. SCHMALHORST 1988 *Journal of Vibration, Acoustics, Stress, and Reliability in Design* **110**, 158–164. Crack depth analysis of a rotating shaft by vibration measurement.
13. H. KEINER and M. S. GADALA 1999 *Proceedings of the* 1*st Canadian Conference on Nonlinear Solid Mechanics*, *Victoria*, *Canada*, 366–374. 3-D finite element analysis of a cracked rotor.
14. A. S. SEKHAR and B. S. PRABHU 1998 *Mechanical Machinery Theory* **33**, 1167–1175. Condition monitoring of cracked rotors through transient response.

15. A. S. SEKHAR and P. BALAJI PRASAD 1997 *Journal of Sound and Vibration* **208**, 457–474. Dynamic analysis of a rotor system considering a slant crack in the shaft.
16. A. S. SEKHAR 1999 *Journal of Sound and Vibration* **233**, 497–512. Vibration characteristics of a cracked rotor with two open cracks.
17. T.-C. TSAI and Y.-Z. WANG 1997 *International Journal of Mechanical Sciences* **39**, 1037–1053. The vibration of a multi-crack rotor.
18. ANSYS, INC. 1999 *ANSYS Rev.* 5.5. Canonsburg, U.S.A.